

Correlated and Individual Multi-Modal Deep Learning for RGB-D Object Recognition

Ziyan Wang
Department of Automation
Tsinghua University
Beijing, China
zy-wang13@
mails.tsinghua.edu.cn

Ruogu Lin
Department of Automation
Tsinghua University
Beijing, China
lrg14@
mails.tsinghua.edu.cn

Jiwen Lu
Department of Automation
Tsinghua University
Beijing, China
lujiwen@
mail.tsinghua.edu.cn

Jianjiang Feng
Department of Automation
Tsinghua University
Beijing, China
jfeng@tsinghua.edu.cn

Jie Zhou
Department of Automation
Tsinghua University
Beijing, China
jzhou@tsinghua.edu.cn

ABSTRACT

In this paper, we propose a new correlated and individual multi-modal deep learning (CIMDL) method for RGB-D object recognition. Unlike most conventional RGB-D object recognition methods which extract features from the RGB and depth channels individually, our CIMDL jointly learns feature representations from raw RGB-D data with a pair of deep neural networks, so that the sharable and modal-specific information can be simultaneously exploited. Specifically, we construct a pair of deep convolutional neural networks (CNNs) for the RGB and depth data, and concatenate them at the top layer of the network with a loss function which learns a new feature space where both correlated part and the individual part of the RGB-D information are well modelled. The parameters of the whole networks are updated by using the back-propagation criterion. Experimental results on two widely used RGB-D object image benchmark datasets clearly show that our method outperforms state-of-the-arts.

Keywords

Deep learning, multi-modal learning, RGB-D object recognition

1. INTRODUCTION

Object recognition is one of the most challenging problems in computer vision. With the development of high-quality consumer depth cameras such as the Microsoft Kinect, numerous efforts have been made for RGB-D object recognition in recent years. Compared to RGB object recognition,

the introduction of depth images greatly improves the recognition performance because depth information provides geometrical cues which are invariant to lighting and color variations, which are usually difficult to describe in conventional RGB images. As there is a growing trend of the appearance of many depth-camera embedded devices like Google Tango [1] and Microsoft Hololens [2], the requirements and application potentials for RGB-D object recognition technology are growing rapidly.

There are two main procedures in RGB-D object recognition: feature representation [3, 4, 34, 35] and object matching [11, 15, 23]. Compared with object matching, feature representation affects the performance of the objective recognition system significantly, because real-world objects usually suffer from large intra-class discrepancy and inter-class affinity. A variety of methods have been proposed for RGB-D object representation recently, and they can be mainly classified into two categories: hand-crafted methods and learning-based methods. Methods in the first category design an elaborated hand-crafted descriptor for both the RGB and depth channels [6, 9, 29] for feature extraction. Representative features include textons [34], color histograms [3], SIFT [35] and SURF [4], which describe objects from different aspects such as color, shape, and texture. However, these methods usually require large amount of strong domain-specific knowledge, which are inconvenient to generalize to different datasets. Methods in the second category employ some machine learning techniques to learn feature representations in a data-driven manner, so that more data-adaptive discriminative information can be exploited [5, 8, 30, 44, 48]. However, most existing learning-based methods consider the RGB and depth information from two different channels individually, which ignore the sharable property and the interaction relationship between these two modalities. To address this, Wang *et al.* [48] proposed a multi-modal learning approach by extracting RGB and depth features within the deep learning framework, which can fully exploit the information of both RGB and depth modalities. While the correlation information of the RGB and depth information can be exploited, the modal-specific information has been ignored in their method, so that the individual part is contaminated

by the correlated part which harms the discriminative power of the learned features. Moreover, they treat the individual part and correlated part equally, which neglects the different discriminative power between them.

In this paper, we propose a correlated and individual multi-modal deep learning (CIMDL) method for RGB-D object recognition. Specifically, we develop a multi-modal learning framework to learn discriminative features from both the correlated and individual parts, and automatically learn the weights for different feature components in a data-driven manner. The basic pipeline of our proposed CIMDL is illustrated in Figure 1. We first utilize two ways of deep CNNs to learn features from RGB and depth modality individually. Then, we feed the features learned from these two channels into a multi-modal learning layer to concatenate them. This layer is designed for three purposes: 1) generating the correlated part between these two modalities; 2) extracting the discriminative part of features from both of these two modalities; 3) learning the weights for the correlated and individual parts automatically for feature combination. Finally, a feature vector containing both the correlated part and the individual part of the RGB and depth modalities is obtained at the top layer of the network, which is used as the final feature representation for RGB-D object recognition. The parameters of the whole network are updated by using the back-propagation criterion. Experimental results on the RGB-D object [29] and 2D3D [9] datasets are presented to show the effectiveness of the proposed approach.

2. RELATED WORK

2.1 RGB-D Object Recognition

Most conventional RGB-D object recognition methods use hand-crafted feature descriptors for object matching. For example, Lai *et al.* [29] exploited a bunch of hand-crafted features including color histograms [3], textons [34] and SIFT [35] for RGB channel, spin images [27] and SIFT [35], and multiple shape features for the depth channel for feature representation. Finally, they concatenated these features together as the final representation for recognition. Bo *et al.* proposed a kernel descriptor method [6] which combines several RGB-D image features such as 3D shape features, depth edge features and texture features for RGB-D object recognition.

In recent years, learning-based features have aroused more and more attention in RGB-D object recognition. For example, Blum *et al.* [5] identified interesting points by using the SURF method and clustered patches around them with a unsupervised learning method to obtain a codebook for feature encoding. Bo *et al.* [7] presented a Hierarchical Matching Pursuit (HMP) method to learn advanced representations from local patches. Socher *et al.* [44] presented a cascaded network by integrating convolutional neural networks and recursive neural networks, which first learned color and depth features individually and then combined them into a concatenated feature vector. The single-layer convolutional network was trained first and the output was used as the input of the recursive network, which ensures that different levels of features can be learned by different parts of the whole network. Browazki *et al.* [9] fused several SVMs-trained features by utilizing a multi-layer perception. Lai *et al.* [30] devised an distance metric learning approach [36, 42] to fuse heterogeneous feature representations for RGB-D ob-

ject recognition. However, most of them learn features from the color and depth channels individually, and construct a final representation by a simple concatenation, which usually ignores the physical meanings of different modalities of features and their potential relationship.

2.2 Deep Learning

Deep learning has achieved encouraging performance on a variety of computer vision applications, and outperforms many state-of-the-arts in various visual analysis tasks. Representative deep models include stack auto-encoder [37, 47], deep Boltzmann machine [40, 41], convolutional neural network [32], recursive neural network [50], and long short term memory unit [10]. These methods can address the limitations of hand-crafted features so that they can be easily adapted to datasets because only raw data are required for feature learning. Among these deep learning methods, convolutional neural networks (CNN) have showed excellent performance on various computer vision tasks such as object recognition [21, 22, 28], object detection [17, 18, 43], scene labeling [16], face verification [24, 46], action recognition [25] and visual object tracking [20, 38].

Deep learning has also been employed for RGB-D visual analysis in recent years. For example, Gupta *et al.* [19] proposed an approach to encode the depth data into three channels: horizontal disparity, height above ground, angle between point normal and inferred gravity. Then, they trained CNNs on these three-channel instead of the ordinal depth images for RGB-D object recognition and segmentation. Couprie *et al.* [12] presented a multi-scale CNN for RGB-D scene labeling based on a hierarchical feature method [16]. Wang *et al.* [49] designed a deep neural network for surface normal prediction. However, these methods ignored the relationship between data from different modalities because the RGB and depth information are only simply concatenated.

More recently, several multi-modal deep learning methods have been proposed to make better use of the RGB and depth information for various visual analysis tasks. For example, Srivastava *et al.* [45] proposed a multi-modal Deep Boltzmann Machine approach, where a concatenated layer was added to connect DBMs from different modalities to learn multi-modal feature representations jointly. Eitel *et al.* [14] proposed a two-stream CNN model combined with a fusion layer for RGB-D object recognition. Wang *et al.* [48] proposed a multi-modal feature deep learning approach by exploiting the shared properties of RGB and depth images for RGB-D object recognition. Lenz *et al.* [33] presented a multi-modal deep learning approach for robotic grasp detection, where the stacked auto-encoders were used for multi-modal feature learning.

3. PROPOSED APPROACH

3.1 Baseline Architecture

Several ways of CNN-based methods have been proposed for RGB-D object recognition. For example, Couprie *et al.* used a four-channel CNNs (three are from the RGB data and the other one is from the depth data) for scene labeling [12]. Gupta *et al.* [19] extracted features from RGB and depth images independently and concatenated them as the final features for object detection, where both the RGB CNN and the depth CNN are fine-tuned on the model which was pre-

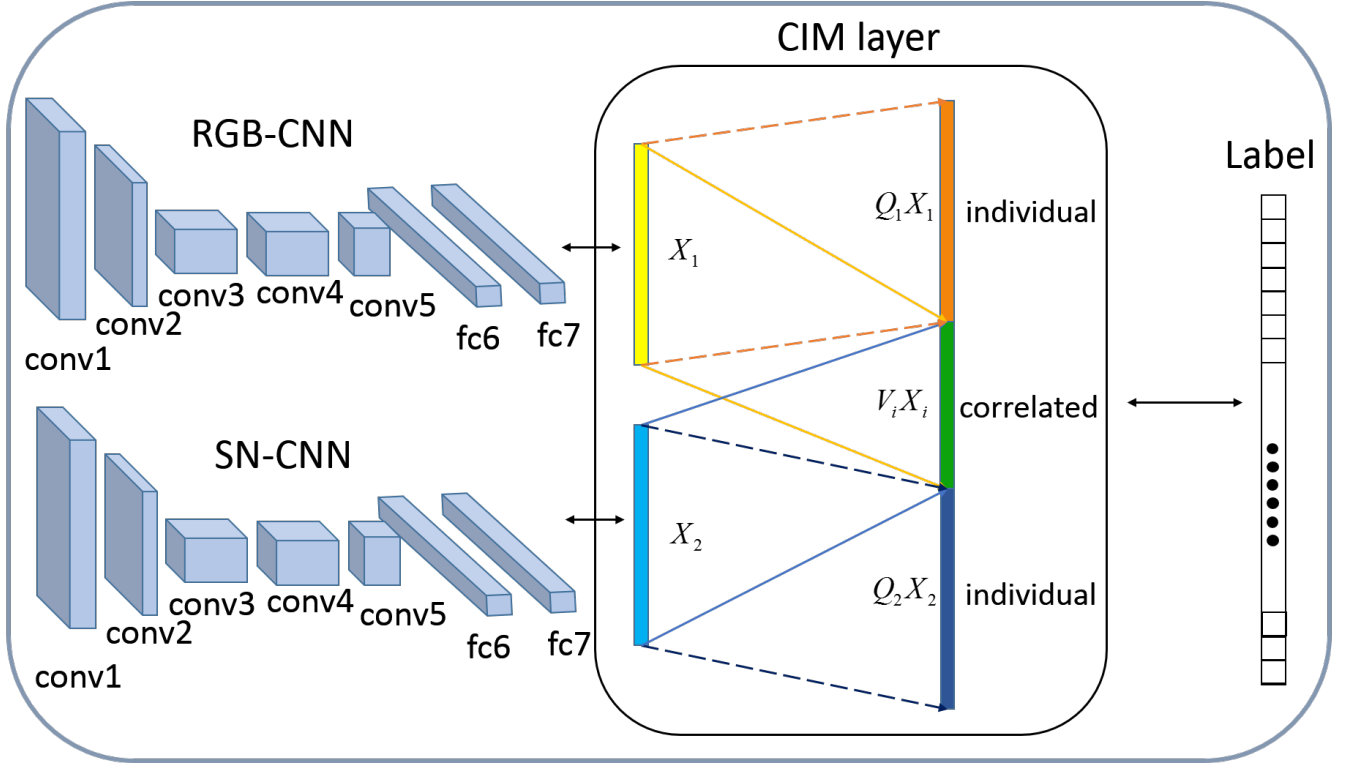


Figure 1: The pipeline of our proposed approach. We construct a two-way CNN for RGB images and surface normal depth images for feature extraction. We design a multi-modal learning layer to learn the correlated part V_iX_i and the individual parts Q_iX_i of the RGB and depth features, respectively. We project the RGB-D features X_1, X_2 into a new feature space. The loss function enforces the affinity of the correlated part from different modalities and discriminative information of the modal-specific part, where the combination weights are also automatically learned within the same framework. Here 'conv' and 'fc' represents the 'convolutional layer' and the 'fully connected layer', respectively. (best view in the color file)

trained on the ImageNet dataset [13]. Another method is to fuse the second fully connected layer of the RGB network and the depth network so that the supervised information can be back-propagated for both modalities. These models are shown in Figure 2. The structure of the CIMDL layer which we used in this work is shown in Figure 3. We have 5 convolution layers and 3 fully connected layers. To build a baseline architecture, we train the networks independently by following the setting in [19] to extract features vectors from the fc7 layer. For the depth network, we adopt the surface normals for the network training, which can be finetuned on the RGB pre-trained model.

3.2 Multi-modal Learning Model

We develop a multi-modal deep architecture for RGB-D feature learning, which consists of two convolutional neural networks. Specifically, we adopt two models which were pre-trained on the ImageNet dataset [13] and finetune them on our RGB training dataset and the depth training dataset to generate the parameters of RGB-CNN and SN-CNN layers, respectively. Then, we feed the outputs of the second fully connected layer from both RGB-CNN and SN-CNN into our correlated and individual multi-modal learning structure. In our new structure, we replace the original softmax layer with our new CIMDL layer which will be detailed later. The pipeline of our proposed method is shown in Figure 3. In-

stead of directly putting the depth image to the CNN network, we also extract the surface normal of the depth information by following the setting in [19], which encodes it as a three-channels representation. We empirically find that the surface normal results in better recognition performance than the raw depth data in feature learning.

Figure 3 shows the architecture of the last layer of our network, where $X_i = [x_{i1}, x_{i2}, \dots, x_{iN}] \in \mathbf{R}^{M \times N}$ denote the activations of the second fully connected layer of RGB-CNN and SN-CNN with N images in one data batch, $Q_i, V_i \in \mathbf{R}^{M \times M}$ are mapping matrices which transfer original features into the modal-specific domain and the correlated domain, and $L \in \mathbf{R}^{l \times N}$ denotes the label matrix with l classes.

The physical meaning of our multi-modal learning model is to leverage the correlated properties of the RGB and depth information, and enforce the modal-specific property of both modalities and adjust the weights for different parts of the feature in recognition. Therefore, the final purpose of the proposed method is to learn two mapping matrices V and Q to map the original feature into the correlated feature space and the individual feature space. Hence, there are three key characteristics in our model: 1) a multi-modal deep learning strategy which can automatically decompose features into a correlated part and an individual part; 2) ensuring the discriminative power and orthogonality of correlated part and individual part; and 3) learning the weights for different

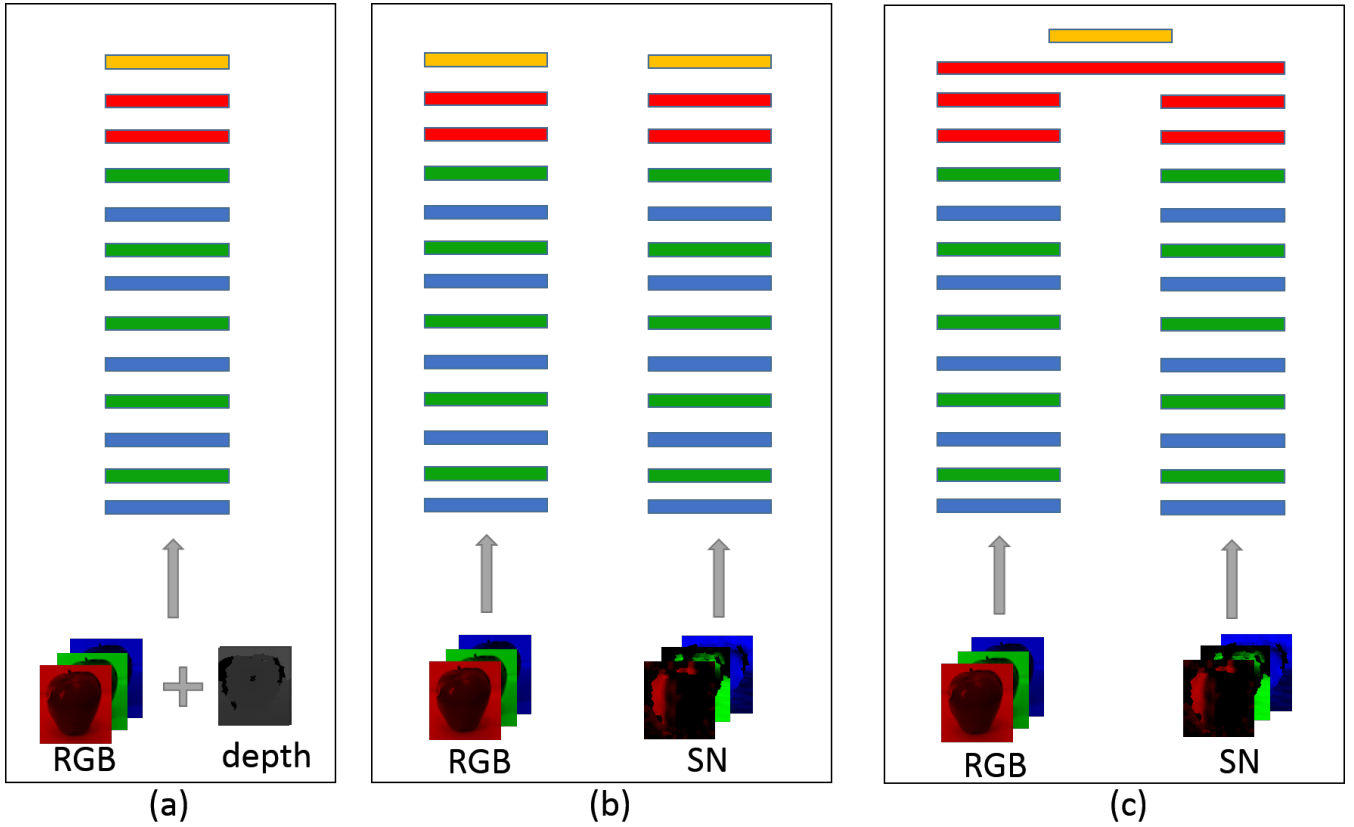


Figure 2: Three kinds of CNN architectures for RGB-D feature extraction. For each network, each rectangle represents a layer and the color indicates the layer’s identity. The followings rules are: blue - convolutional; green - pooling; red - fully connected; yellow - softmax. (best view in the color file)

parts in a data-driven manner to improve the recognition performance.

3.3 Objective Function

Given two datasets, we first learn the mapping matrices $V_i (i = 1, 2)$ for both modalities to map the original features into the correlated feature space, where we expect to minimize the difference between the correlated parts from two datasets, respectively. Let $X_i \in \mathbf{R}^{M \times N}$ be the M -dimensional activations of the second fully connected layer in one batch with N images, where $i = 1, 2$ corresponds to the RGB channel and depth channel, respectively. Our goal is to learn discriminative feature representations to achieve two objectives: 1) some information are shared by different modalities, and 2) some modal-specific information are exploited for each modality individually. To achieve this, we formulate the following objective function:

$$\min_{V_1, V_2} \|V_1 X_1 - V_2 X_2\|_F^2 \quad (1)$$

where $\|\cdot\|_F$ denotes the Frobenius norm. By minimize the above objective function, the mapping matrix will eventually guarantee the similarity of correlated part from both modalities. Besides the correlated part, the modal-specific feature is also an essential part of the feature $X_i (i = 1, 2)$. Hence, we present the following criterion to ensure this ob-

jective:

$$X_i = C_i + A_i (i = 1, 2) \quad (2)$$

where C_i is the correlated part and A_i denotes the modal-specific components of the i th modality’s feature. The correlated part is the component of the original feature X_i . Both the correlated feature and model-specific feature reconstruct the original feature as follows:

$$C_i = V_i^T V_i X_i (i = 1, 2) \quad (3)$$

$$A_i = Q_i^T Q_i X_i (i = 1, 2) \quad (4)$$

where $V_i \in \mathbf{R}^{M \times M}$ is the mapping matrix to project the original feature into the correlated domain and $Q_i X_i$ denotes the individual component of the i th modality’s feature. Since these two matrices V_i, Q_i map the original feature into the correlated domain and the modal-specific domain, respectively, they should be unrelated and not contaminated by each other. Therefore, the mapping matrices contains bases that come from discrepant space and should be orthogonal to each other. Therefore, we present the following constraints:

$$V_i^T Q_i = 0, (i = 1, 2) \quad (5)$$

Consequently, we formulate the objective function of our multi-modal feature learning as two parts. The first part enforces the features of two domains to share a congruity part after the mapping V . The second part is the softmax

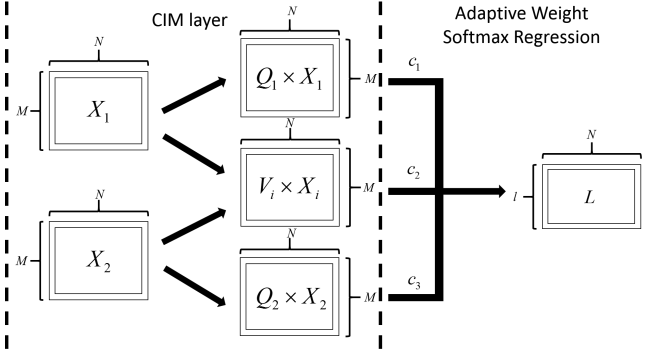


Figure 3: The architecture of the last layer of our network, where V_i, Q_i denotes the mapping matrices that map the original feature into a correlated and individual feature space. The output of the last layer is concatenated into a new feature vector which is assigned with different weights c_i for different components in the learning framework.

loss of our network. The first constraint ensures the reconstruction of the original feature, and the second constraint engenders discrepancy between the correlated part and the modal-specific part.

$$\begin{aligned} & \min_{V_1, V_2, Q_1, Q_2} \|V_1 X_1 - V_2 X_2\|_F^2 \\ & + \mu \mathcal{L}(\text{softmax}(W, T, L, c)), \\ \text{s.t. } & X_i = V_1^T V_i X_i + Q_1^T Q_i X_i, (i = 1, 2) \\ & V_i^T Q_i = 0, (i = 1, 2) \end{aligned} \quad (6)$$

where $W = [W_1, W_2, W_3]$, $W_i \in \mathbf{R}^{l \times M}$ are the weights of the last softmax layer for different modalities, T is the activation of the CIMDL layer. In Figure 3, the matrices in the middle show the detail of T . c is weight for different parts of the feature T for softmax regression which will be introduced later. Here we incorporate supervised learning by minimize the loss of softmax regression from WT to L .

3.4 Optimization

In this work, we adopt an alternating optimization for all those variables V_i, Q_i, W, c . Following the Lagrange Multiplier and Gradient Decent criterion, we easily obtain a local optimal solution for (5). Based on (5), we construct a Lagrange function as follows:

$$\begin{aligned} \mathcal{L}(\alpha, \sigma, \delta, \theta, \mu) = & \|V_1 X_1 - V_2 X_2\|_F^2 \\ & + \sum_{i=1,2} \alpha_i \|X_i - V_i^T V_i X_i - Q_i^T Q_i X_i\|_F^2 \\ & + \sum_{i=1,2} \sigma_i \|V_i^T Q_i\|_F^2 \\ & + \sum_{i=1,2} \delta_i g(V_i X_i) + \theta_i g(Q_i X_i) \\ & + \mu h(WT - L) + \eta \|W\|_{2,1} \end{aligned} \quad (7)$$

where $\|\cdot\|_F$ denotes the Frobenius norm. α_i and σ_i are positive Lagrange multipliers associated with the linear constraints $X_i = V_i^T V_i X_i + Q_i^T Q_i X_i$ and $V_i^T Q_i = 0$. The

first term of the objective function intends to minimize the difference of the correlated part that generated from the color modality and the depth modality separately. The second term regulated the feature's ability to be reconstructed by its correlated part and modal-specific part. The third part ensures the mutual orthogonality by regulating the inner product of the two transfer matrix V_i and Q_i . The last part of the objective function is regularization of $V_i X_i$ and $Q_i X_i$ where $g(\cdot) = \log(\cosh(\cdot))$ denotes the smooth L_1 penalty function [31].

By applying the conventional gradient decent algorithm, we update the variables V_i, Q_i, W with the same learning rate. First, we update V_i, Q_i . The derivative of the Lagrange function $\mathcal{L}(\alpha, \sigma, \delta, \theta, \mu)$ with respect to V_1 can be expressed as

$$\begin{aligned} \frac{\partial \mathcal{L}}{\partial V_1} = & 2[(V_1 X_1 - V_2 X_2) X_1^T + \sigma_1 Q_1 Q_1^T V_1 \\ & - 2\alpha_1 V_1 X_1 (X_1 - V_1^T V_1 X_1 - Q_1^T Q_1 X_1)^T \\ & + \delta_1 g'(V_1 X_1) \\ & + 0.5\mu c_1 W_1^T (L - P) X_1^T] \end{aligned} \quad (8)$$

where $g'(\cdot)$ is the derived function of smooth L_1 penalty function. c_1 is the weight of the correlated part in the regression.

$$\begin{aligned} P = & \exp(-[c_1 W_1, c_2 W_2, c_3 W_3] \\ & \times [\frac{V_1 X_1 + V_2 X_2}{2}, Q_1 X_1, Q_2 X_2]) \end{aligned} \quad (9)$$

According to the gradient descent rule, V_1 is updated as

$$V_1[t+1] = V_1[t] - \gamma \frac{\partial \mathcal{L}}{\partial V_1[t]} \quad (10)$$

For V_2 , we have the derivative of the Lagrange function $\mathcal{L}(\alpha, \sigma, \delta, \theta, \mu)$ with respect to V_2 as

$$\begin{aligned} \frac{\partial \mathcal{L}}{\partial V_2} = & 2[(V_2 X_2 - V_1 X_1) X_2^T + \sigma_2 Q_2 Q_2^T V_2 \\ & - 2\alpha_2 V_2 X_2 (X_2 - V_2^T V_2 X_2 - Q_2^T Q_2 X_2)^T \\ & + \delta_2 g'(V_2 X_2) \\ & + 0.5\mu c_1 W_2^T (L - P) X_2^T] \end{aligned} \quad (11)$$

According to the gradient descent rule, V_2 is updated as:

$$V_2[t+1] = V_2[t] - \gamma \frac{\partial \mathcal{L}}{\partial V_2[t]} \quad (12)$$

The derivative of the Lagrange function $\mathcal{L}(\alpha, \sigma, \delta, \theta, \mu)$ with respect to Q_1 can be expressed as

$$\begin{aligned} \frac{\partial \mathcal{L}}{\partial Q_1} = & 2[-\alpha_1 Q_1 X_1 (X_1 - V_1^T V_1 X_1 - Q_1^T Q_1 X_1)^T \\ & + \sigma_1 V_1 V_1^T Q_1 + \theta_1 g'(Q_1 X_1) \\ & + \mu c_2 W_2^T (L - P) * X_1^T] \end{aligned} \quad (13)$$

According to the gradient descent rule, Q_1 is updated as

$$Q_1[t+1] = Q_1[t] - \gamma \frac{\partial \mathcal{L}}{\partial Q_1[t]} \quad (14)$$

The derivative of the Lagrange function $\mathcal{L}(\alpha, \sigma, \delta, \theta, \mu)$ with

Algorithm 1 : CIMDL

Input: Training set from both modality $\mathbf{X}_1, \mathbf{X}_2$, ground truth label matrix \mathbf{L}

Output: Mapping matrix $\mathbf{V}_i, \mathbf{Q}_i (i = 1, 2)$, projection matrix $\mathbf{W} = [\mathbf{W}_1, \mathbf{W}_2, \mathbf{W}_3]$, adaptive weights $\mathbf{c} = [\mathbf{c}_1, \mathbf{c}_2, \mathbf{c}_3]$

```

1: Initialize  $\mathbf{W}, \mathbf{V}_1, \mathbf{V}_2, \mathbf{Q}_1, \mathbf{Q}_2, \mathbf{c}$ 
2: while not converge do
3:   Fix  $\mathbf{W}, \mathbf{c}$ ,
4:   Update  $\mathbf{V}_1, \mathbf{V}_2$  according to (9) and (11).
5:   Fix  $\mathbf{W}, \mathbf{c}$ ,
6:   Update  $\mathbf{Q}_1, \mathbf{Q}_2$  according to (13) and (15).
7:   Fix  $\mathbf{V}_1, \mathbf{V}_2, \mathbf{Q}_1, \mathbf{Q}_2, \mathbf{c}$ ,
8:   Update  $\mathbf{W}$  according to (17)
9:   Fix  $\mathbf{V}_1, \mathbf{V}_2, \mathbf{Q}_1, \mathbf{Q}_2, \mathbf{W}$ ,
10:  Update  $\mathbf{c}$  according to (18)
11: end while
12: return  $\mathbf{W}, \mathbf{V}_1, \mathbf{V}_2, \mathbf{Q}_1, \mathbf{Q}_2, \mathbf{c}$ 

```

respect to Q_2 can be expressed as:

$$\begin{aligned} \frac{\partial \mathcal{L}}{\partial Q_2} = & 2[-\alpha_2 Q_2 X_2 (X_2 - V_2^T V_2 X_2 - Q_2^T Q_2 X_2)^T \\ & + \sigma_2 V_2 V_2^T Q_2 + \theta_2 g'(Q_2 X_2) \\ & + \mu c_3 W_3^T (L - P) * X_2^T] \end{aligned} \quad (15)$$

According to the gradient descent rule, Q_2 is updated as

$$Q_2[t+1] = Q_2[t] - \gamma \frac{\partial \mathcal{L}}{\partial Q_2[t]} \quad (16)$$

Having completed updating the mapping matrices V_i and Q_i , we keep them fixed and update the regression matrix W . According to the work of [39], the derivative of the Lagrange function $\mathcal{L}(\alpha, \sigma, \delta, \theta, \mu)$ with respect to W is

$$\frac{\partial \mathcal{L}}{\partial W} = 2(\mu(L - P)T^T + \eta EW) \quad (17)$$

where E is a diagonal matrix with $e_{jj} = 0.5\|w_j\|_2$, $W = [w_1, w_2, \dots, w_M]$ and $w_i \in \mathbf{R}^{l \times 1}$, $i = \{1, 2, \dots, M\}$. According to the gradient descent criterion, we update W by

$$W[t+1] = W[t] - \gamma \frac{\partial \mathcal{L}}{\partial W[t]} \quad (18)$$

The correlated part of two distinct dataset feature plays a significant part in extracting the shareable information but not equally powerful as the modal-specific part. Therefore, we design adaptive weights for different part of the fused feature. c_1, c_2, c_3 correspond for the correlated part, the modal-specific part for RGB and the modal-specific part for surface normal respectively. With the feature representation of W, V_i, Q_i updated and fixed, we update the adaptive parameter c according to the following rules:

$$c_1 = \|\exp(-W_1 * (V_1 X_1 + V_2 X_2)) - L\|_F^p \quad (19)$$

$$c_2 = \|\exp(-W_2 * Q_1 X_1) - L\|_F^p \quad (20)$$

$$c_3 = \|\exp(-W_3 * Q_2 X_2) - L\|_F^p \quad (21)$$

We regularize the vector $c = [c_1, c_2, c_3]$ and make sure that $c_1 + c_2 + c_3 = 1$. Iteratively, we automatically select the weights for different parts of our learned feature. Our proposed CIMDL method is summarized in **Algorithm 1**.

4. EXPERIMENTS

We conduct experiments on two datasets including the RGB-D Object Datasets [29] and the 2D3D Dataset [9] for RGB-D object recognition, to evaluate the effectiveness of our proposed method. The followings describe the detailed experimental settings and results.

4.1 Datasets

RGB-D Object Dataset: The RGB-D dataset is a large dataset containing 51 different classes of 300 distinct objects shoot from multiple views. The objects in this dataset are cups, fruits, households, tools, vegetables, things that occurred frequently in daily life and commonplace. Each of them is recorded by cameras located at three different positions in the video mode. There are 207,920 RGB-D image frames, with roughly 600 images per object. In our experiments, we conduct a down-sampling from every 5 consecutive frames of the video. We run the 10 random splits provided by [29], where each of those splits covers the whole 51 classes with different objects. Finally, it came out with approximately 51 different test objects. We conduct experiments on those different splits, where there are 34000 images in average for training and 6900 images in average for testing.

2D3D Dataset: The 2D3D dataset includes 154 objects in 14 different classes. Those objects includes books, bottles, monitors that occurred frequently in office. Each of them is recorded by a *PMDTM* CamCube 2.0 time-of-flight camera, generating 5544 RGB-D images in total which were shot in different evaluation angles. Following the same settings in [9], we divided the dataset into the training part and the testing part, containing 6 objects of each class. Finally, 1476 RGB-D images from 82 objects are used for training and 1332 RGB-D images from 74 objects are employed for testing.

4.2 Implementat Details

Architecture of CNNs: Our experiments were performed on the Caffe framework [26]. We adopted the same R-CNN structure as in [18] and [19]. We modified the input layer for the 3-channels image input instead of bounding boxes. The two modalities shared the same network architecture before the fc7 layer. For both the RGB modality and the surface normal modality, the input images were resized to $227 \times 227 \times 3$. The convolutional kernel of the conv1 layer was set as $11 \times 11 \times 96$ with a stride of 4. The kernel of conv2 is set was $5 \times 5 \times 256$ with a pad of 2. The kernel of conv3 was set as $3 \times 3 \times 384$ with a pad of 1. The kernel of conv4 was set as $3 \times 3 \times 384$ with a pad of 1. The kernel of conv5 was set as $3 \times 3 \times 256$ with a pad of 1. Stride for conv2 and conv5 were set as 2. The size of fully connected layer's output was 4096 for both the fc6 and fc7 layers. Both of the two fully connected layers were followed by a dropout layer with a dropout rate of 0.5. Max pooling was applied on the conv1, conv2 and conv5 layers, and there are ReLU non-linearity layers [28] for every convolutional layers and fully connected layers.

Finetuning: The R-CNN model was pre-trained on the ImageNet dataset [13] both for RGB and SN channels. Our finetuning setting is the same as the one used in [19], where the learning rate was initialized at 0.001 and decreased by a factor of 10 every 10,000 iterations. We finetuned the model with 30,000 iterations. The whole finetuning part was done

by a GTX TITAN X and it took nearly 3 hours for the whole finetuning procedure.

Parameters Setting: In the Lagrange function of our multi-modal learning model, α and σ are the reconstruction and orthogonal controlling parameters, and they were set as follows: $\{\alpha_i = \frac{0.5}{N} | i = 1, 2\}$ and $\{\sigma_i = \frac{0.5}{M} | i = 1, 2\}$, where N denotes the size of training samples and M denotes the size of the feature vectors, μ is the softmax regression controlling parameter and it is set as $\frac{10}{N}$. δ, θ, η are regularization parameters and they were empirically set as $\{\delta_i = \frac{0.005}{N} | i = 1, 2\}$, $\{\theta_i = \frac{0.005}{N} | i = 1, 2\}$ and $\eta = 1$, the learning rate for W is set empirically as 10^{-3} and for V_i, Q_i as 10^{-5} , respectively. All parameters were set the same for experiments both on RGB-D object dataset and 2D3D dataset.

4.3 Results on RGB-D Object Dataset

Comparison with Existing Deep Learning Baselines: We first constructed several deep learning baselines for RGB-D object recognition by using CNN and compared them with our proposed approach. Motivated by the work of Gupta *et al.*[19] and Eitel *et al.*[14], we encoded each depth image into surface normal to efficiently exploit the information provided by depth image.

The structure of our different baseline methods are detailed as follows: 1) CNN using only RGB image as input with and without pretrain; 2) CNN using only depth images as input; 3) CNN using only surface normal images as input with and without pretrain; 4) CNN using RGB and depth image as a 4-channel input; 5) CNN using RGB and surface normal as a 6-channel input; 6) two separate ways of CNN trained for RGB and depth with fc7 concatenated; and 7) two separate ways of CNN trained for RGB and surface normal with fc7 concatenated, with and without pretrain.

Table 2 shows the performance of different baselines. We see that the CNN trained by raw depth images achieves worse performance than that trained by the surface normal. This is because surface normal can better represent geometry information than depth images. The accuracy rises swiftly when we combine the RGB and depth image into a 4-channel input. RGB-SN 6-channel input performs a comparative result with RGB-D 4-channel input CNN. This indicates that the addition of more modalities improves the recognition performance than only using one modality such as RGB or depth image. However, the performance of the architecture which fuses the RGB and depth image from the input degenerates the modal-specific part of different input modality greatly. The experimental results clearly shows that the two way CNN structure prone to be more effective and accurate with more information from modal-specific part.

In order to boost performance on the RGB-D object dataset, we also used the caffe model pre-trained on the ImageNet [13] for both RGB input CNN and SN input CNN. In contrast with the same structure without pretrain model, we have achieved much better result on accuracy.

Table 3 shows the comparison between the results of our proposed CIMDL method and the best baselines which use two ways of CNN(RGB CNN and SN CNN) with pretrained models and concatenated at the fc7 layer of the two CNN. In our method, we use surface normal as a substitute of the depth image with pretrained model. Our proposed multi-modal learning method outperforms the best baseline by

Table 1: Comparison of our method and state-of-the-arts methods on the RGB-D object dataset.

Method	Accuracy (%)
Lai <i>et al.</i> [29]	81.9 ± 2.8
Blum <i>et al.</i> [5]	86.4 ± 2.3
Socher <i>et al.</i> [44]	86.8 ± 3.3
Bo <i>et al.</i> [8]	87.5 ± 2.9
Wang <i>et al.</i> [48]	88.5 ± 2.2
Ours	89.6 ± 2.1

Table 2: Comparison of our method and the compared deep learning baselines.

Method	Accuracy (%)
RGB CNN	74.6 ± 2.9
Depth CNN	75.5 ± 2.7
SN CNN	76.3 ± 2.5
RGB-D 4-channel CNN	80.2 ± 1.9
RGB-SN 6-channel CNN	80.7 ± 2.1
RGB CNN (pretrain)	82.7 ± 2.4
SN CNN (pretrain)	85.2 ± 2.1
RGB-Depth CNN with fc7 concat	84.7 ± 2.1
RGB-SN CNN with fc7 concat	85.0 ± 2.4
RGB-SN CNN with fc7 concat (pretrain)	87.8 ± 2.3
Ours	89.6 ± 2.1

1.8% in accuracy. Comparing to the best baseline that simply connect the fc7 layer, our method can 1) generate the correlated part and the modal-specific part of different modalities and make sure they are not contaminated by each other 2) better exploit the information from the correlated and individual part of different modalities.

Comparison with State-of-the-arts: We also compare our method with four state-of-the-art RGB-D object recognition methods: 1) extracting depth feature using SIFT and spin images, RGB image using SIFT and color and texon histogram [29]; 2) using convolutional k-means descriptor [5]; 3) Recursive Neural Network combined with CNN [44]; and 4) MMSS [48]. Table 1 shows that our method outperformed all the state-of-the-arts. We clearly see that our methods outperforms existing state-of-the-arts.

Figure 4 shows the confusion matrix of recognition results on RGB-D object dataset. The diagonal elements represent the accuracy for each object class. We display several misclassified objects and challenging pairs in Figure 5. Those error dues to the similarity objects from different classes like camera and cellphone or color affinity of ball and garlic. Texture similarity is also to be blamed for misclassification.

4.4 Results on 2D3D Dataset

We utilized the same architecture in Sec 4.3 and use the

Table 3: Comparison of our method with the best deep learning baseline.

Method	Accuracy (%)
RGB-SN CNN with fc7 concat + softmax	87.8 ± 2.3
Ours	89.6 ± 2.1

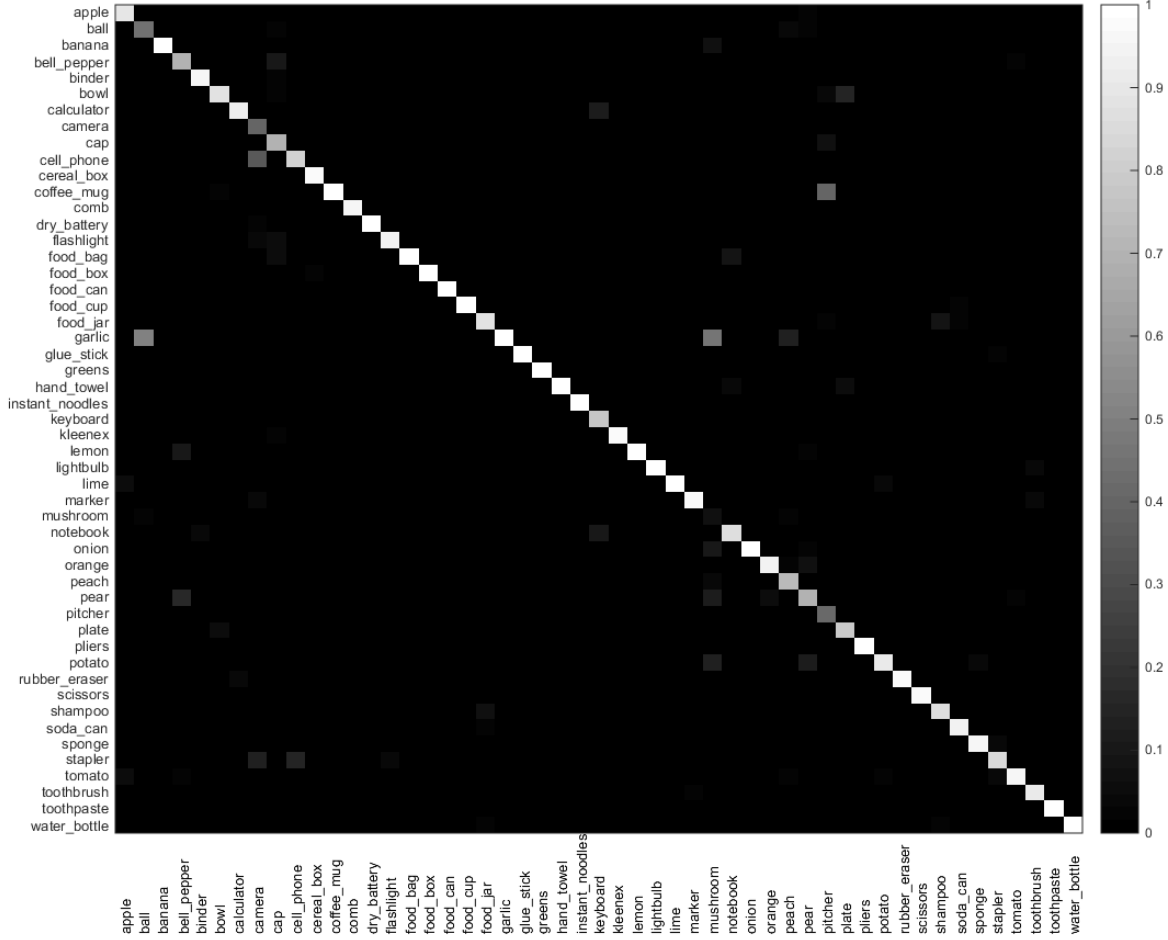


Figure 4: The confusion matrix of our method on the RGB-D object dataset, where the vertical axis indicates the ground truth label and the horizontal axis indicate the predicted label, respectively.

Table 4: Comparison with state-of-the-art methods on the 2D3D dataset.

Method	Accuracy(%)
Browatzki <i>et al.</i> [9]	82.8
Bo <i>et al.</i> [8]	91.0
Wang <i>et al.</i> [48]	91.3
Ours	92.9

same pre-trained caffe model. Table 4 shows the comparison between our proposed method and several state-of-the-art methods. The confusion matrix of our recognition results are shown in Figure 6.

4.5 Parameter Analysis

The accuracy of our object recognition method is affected by the weights c_i ($i = 1, 2, 3$), which decides whether the correlated component or the modal-specific part from RGB or depth dominates. In our proposed method, the weights are self-adapted. In this section, we kept the weights c_i ($i = 1, 2, 3$) fixed and revealed the relationship between weights

and the recognition accuracy. Note that c_1 is for the correlated part and c_2, c_3 correspond to the RGB and depth modality, respectively, where we have $\sum_{i=1}^3 c_i = 1, c_i > 0$. We set parameter p as $p = c_1$.

Figure 7 shows the recognition rate of our method versus different values of the weighting parameter p . In Figure 7, when p is small, which means that the correlated part plays smaller significance in recognition and the accuracy is relatively low. When p becomes larger, the correlated part gradually plays a relatively larger important part than p is low, the accuracy rises. However, when p is too large, which means that the correlated part dominates, the accuracy decreases as the effects of the modal-specific part begin to vanish. The value of c reaches the peak is close to the scenario when the parameter c learned by our multi-modal learning method.

5. CONCLUSIONS

In this paper, we have proposed a correlated and individual multi-modal deep learning method for RGB-D object recognition. In our proposed method, we enforced both the

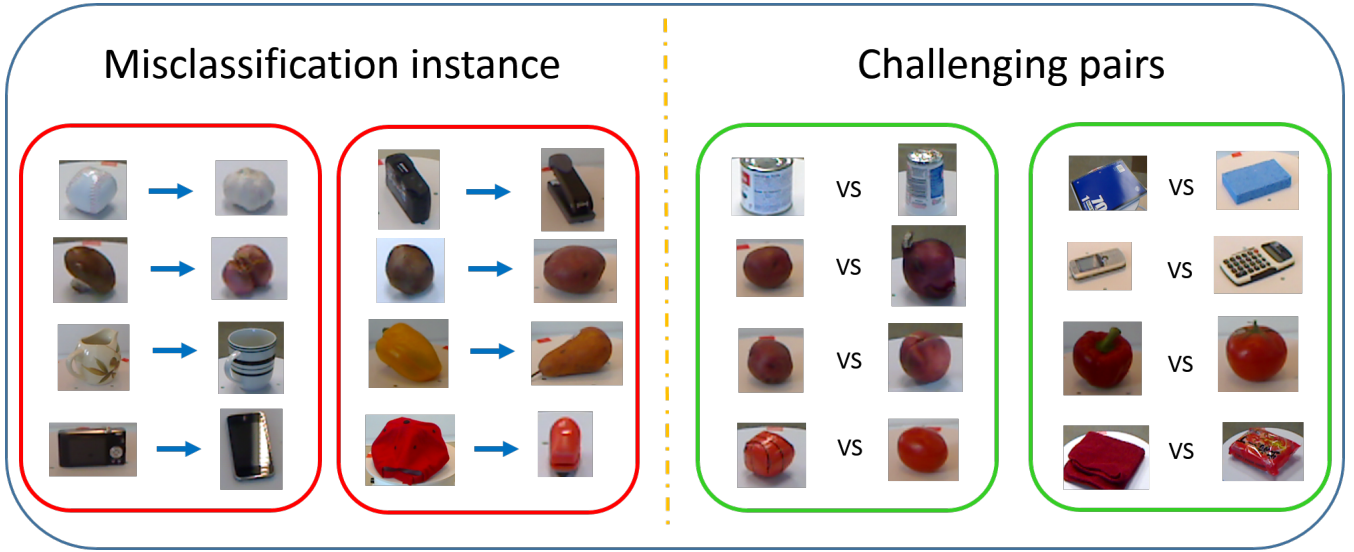


Figure 5: Images on the left side side shows some misclassification instances of our method. Those misclassifications are caused by the large variations of shape, color or texture affinity between objects from other classes. Images on the right side show several challenging pairs, where our methods achieves satisfying results on those pairs even if they have similar shape, texture and color appearances.

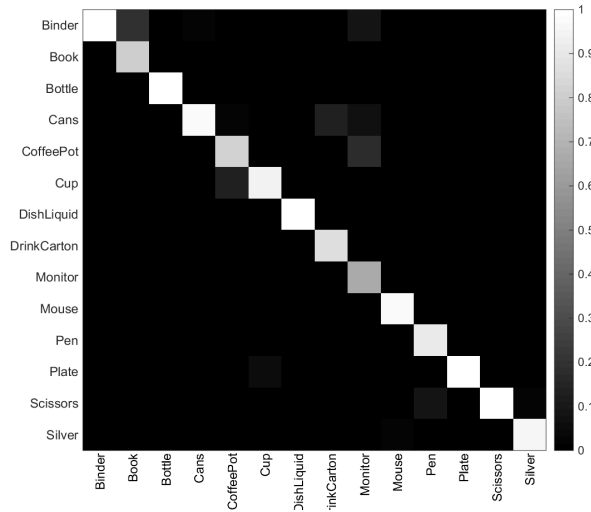


Figure 6: The confusion matrix of our method on the 2D3D dataset, where the vertical axis indicates the ground truth and the horizontal axis indicates the predicted labels, respectively.

correlated and the modal-specific parts in our learned features for RGB-D image object to satisfy several characteristics within a joint learning framework, so that the sharable and modal-specific information can be well exploited. Experimental results on two widely used RGB-D object image benchmark datasets clearly show that our method outperforms state-of-the-arts. How to extend the proposed method for RGB-D video classification seems to be an interesting future direction.

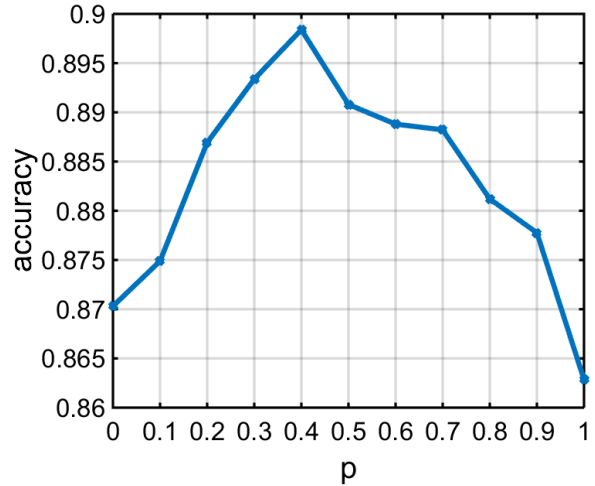


Figure 7: The performance relationship between p and the recognition accuracy on the RGB-D object dataset.

6. REFERENCES

- [1] <https://www.google.com/atap/project-tango/>.
- [2] <https://www.microsoft.com/microsoft-hololens/en-us/>.
- [3] A. E. Abdel-Hakim and A. A. Farag. CSIFT: A SIFT descriptor with color invariant characteristics. In *IEEE Conference on Computer Vision and Pattern Recognition*, pages 1978–1983, 2006.
- [4] H. Bay, A. Ess, T. Tuytelaars, and L. J. V. Gool. Speeded-up robust features (SURF). *Computer Vision and Image Understanding*, 110(3):346–359, 2008.
- [5] M. Blum, J. T. Springenberg, J. Wülfing, and M. A. Riedmiller. A learned feature descriptor for object recognition in RGB-D data. In *IEEE International Conference on Robotics and Automation*, pages 1298–1303, 2012.

- [6] L. Bo, X. Ren, and D. Fox. Depth kernel descriptors for object recognition. In *IEEE/RSJ International Conference on Intelligent Robots and Systems*, pages 821–826, 2011.
- [7] L. Bo, X. Ren, and D. Fox. Hierarchical matching pursuit for image classification: Architecture and fast algorithms. In *Advances in Neural Information Processing Systems*, pages 2115–2123, 2011.
- [8] L. Bo, X. Ren, and D. Fox. Unsupervised feature learning for RGB-D based object recognition. In *International Symposium on Experimental Robotics*, pages 387–402, 2012.
- [9] B. Browatzki, J. Fischer, B. Graf, H. H. Bülthoff, and C. Wallraven. Going into depth: Evaluating 2d and 3d cues for object classification on a new, large-scale object dataset. In *IEEE International Conference on Computer Vision Workshops*, pages 1189–1195, 2011.
- [10] W. Byeon, T. M. Breuel, F. Raue, and M. Liwicki. Scene labeling with LSTM recurrent neural networks. In *IEEE Conference on Computer Vision and Pattern Recognition*, pages 3547–3555, 2015.
- [11] C. Cortes and V. Vapnik. Support-vector networks. *Machine Learning*, 20(3):273–297, 1995.
- [12] C. Couprie, C. Farabet, L. Najman, and Y. LeCun. Indoor semantic segmentation using depth information. *CoRR*, abs/1301.3572, 2013.
- [13] J. Deng, W. Dong, R. Socher, L. Li, K. Li, and F. Li. Imagenet: A large-scale hierarchical image database. In *IEEE Conference on Computer Vision and Pattern Recognition*, pages 248–255, 2009.
- [14] A. Eitel, J. T. Springenberg, L. Spinello, M. A. Riedmiller, and W. Burgard. Multimodal deep learning for robust RGB-D object recognition. In *IEEE/RSJ International Conference on Intelligent Robots and Systems*, pages 681–687, 2015.
- [15] I. M. Elfadel and J. L. W. Jr. The softmax nonlinearity: Derivation using statistical mechanics and useful properties as a multiterminal analog circuit element. In *Advances in Neural Information Processing Systems*, pages 882–887, 1993.
- [16] C. Farabet, C. Couprie, L. Najman, and Y. LeCun. Learning hierarchical features for scene labeling. *IEEE Transactions on Pattern Analysis and Machine Intelligence*, 35(8):1915–1929, 2013.
- [17] R. B. Girshick. Fast R-CNN. *CoRR*, abs/1504.08083, 2015.
- [18] R. B. Girshick, J. Donahue, T. Darrell, and J. Malik. Rich feature hierarchies for accurate object detection and semantic segmentation. In *IEEE Conference on Computer Vision and Pattern Recognition*, pages 580–587, 2014.
- [19] S. Gupta, R. B. Girshick, P. A. Arbeláez, and J. Malik. Learning rich features from RGB-D images for object detection and segmentation. In *European Conference on Computer Vision*, pages 345–360, 2014.
- [20] M. Hahn, S. Chen, and A. Dehghan. Deep tracking: Visual tracking using deep convolutional networks. *CoRR*, abs/1512.03993, 2015.
- [21] K. He, X. Zhang, S. Ren, and J. Sun. Deep residual learning for image recognition. *CoRR*, abs/1512.03385, 2015.
- [22] K. He, X. Zhang, S. Ren, and J. Sun. Spatial pyramid pooling in deep convolutional networks for visual recognition. *IEEE Transactions on Pattern Analysis and Machine Intelligence*, 37(9):1904–1916, 2015.
- [23] T. K. Ho. Random decision forests. In *International Conference on Document Analysis and Recognition*, pages 278–282, 1995.
- [24] J. Hu, J. Lu, and Y.-P. Tan. Discriminative deep metric learning for face verification in the wild. In *IEEE Conference on Computer Vision and Pattern Recognition*, pages 1875–1882, 2014.
- [25] S. Ji, W. Xu, M. Yang, and K. Yu. 3d convolutional neural networks for human action recognition. *IEEE Transactions on Pattern Analysis and Machine Intelligence*, 35(1):221–231, 2013.
- [26] Y. Jia, E. Shelhamer, J. Donahue, S. Karayev, J. Long, R. B. Girshick, S. Guadarrama, and T. Darrell. Caffe: Convolutional architecture for fast feature embedding. In *ACM Multimedia*, pages 675–678, 2014.
- [27] A. E. Johnson and M. Hebert. Using spin images for efficient object recognition in cluttered 3d scenes. *IEEE Transactions on Pattern Analysis and Machine Intelligence*, 21(5):433–449, 1999.
- [28] A. Krizhevsky, I. Sutskever, and G. E. Hinton. Imagenet classification with deep convolutional neural networks. In *Advances in Neural Information Processing Systems*, pages 1106–1114, 2012.
- [29] K. Lai, L. Bo, X. Ren, and D. Fox. A large-scale hierarchical multi-view RGB-D object dataset. In *IEEE International Conference on Robotics and Automation*, pages 1817–1824, 2011.
- [30] K. Lai, L. Bo, X. Ren, and D. Fox. Sparse distance learning for object recognition combining RGB and depth information. In *IEEE International Conference on Robotics and Automation*, pages 4007–4013, 2011.
- [31] Q. V. Le, A. Karpenko, J. Ngiam, and A. Y. Ng. ICA with reconstruction cost for efficient overcomplete feature learning. In *Advances in Neural Information Processing Systems*, pages 1017–1025, 2011.
- [32] Y. LeCun, L. Bottou, Y. Bengio, and P. Haffner. Gradient-based learning applied to document recognition. *Proceedings of the IEEE*, 86(11):2278–2324, 1998.
- [33] I. Lenz, H. Lee, and A. Saxena. Deep learning for detecting robotic grasps. *International Journal of Robotics Research*, 34(4-5):705–724, 2015.
- [34] T. K. Leung and J. Malik. Representing and recognizing the visual appearance of materials using three-dimensional textons. *International Journal of Computer Vision*, 43(1):29–44, 2001.
- [35] D. G. Lowe. Distinctive image features from scale-invariant keypoints. *International Journal of Computer Vision*, 60(2):91–110, 2004.
- [36] T. Malisiewicz and A. A. Efros. Recognition by association via learning per-exemplar distances. In *IEEE Conference on Computer Vision and Pattern Recognition*, 2008.
- [37] J. Masci, U. Meier, D. C. Cireşan, and J. Schmidhuber. Stacked convolutional auto-encoders for hierarchical feature extraction. In *International Conference on Artificial Neural Networks*, pages 52–59, 2011.
- [38] H. Nam and B. Han. Learning multi-domain convolutional neural networks for visual tracking. *CoRR*, abs/1510.07945, 2015.
- [39] F. Nie, H. Huang, X. Cai, and C. H. Q. Ding. Efficient and robust feature selection via joint ℓ_2 , ℓ_1 -norms minimization. In *Advances in Neural Information Processing Systems*, pages 1813–1821, 2010.
- [40] R. Salakhutdinov and G. E. Hinton. Deep boltzmann machines. In *International Conference on Artificial Intelligence and Statistics*, pages 448–455, 2009.
- [41] R. Salakhutdinov and H. Larochelle. Efficient learning of deep boltzmann machines. In *International Conference on Artificial Intelligence and Statistics*, pages 693–700, 2010.
- [42] M. Schultz and T. Joachims. Learning a distance metric from relative comparisons. In *Advances in Neural Information Processing Systems*, pages 41–48, 2003.
- [43] P. Sermanet, D. Eigen, X. Zhang, M. Mathieu, R. Fergus, and Y. LeCun. Overfeat: Integrated recognition, localization and detection using convolutional networks. *CoRR*, abs/1312.6229, 2013.
- [44] R. Socher, B. Huval, B. P. Bath, C. D. Manning, and A. Y. Ng. Convolutional-recursive deep learning for 3d object classification. In *Advances in Neural Information Processing Systems*, pages 665–673, 2012.
- [45] N. Srivastava and R. Salakhutdinov. Multimodal learning with deep boltzmann machines. In *Advances in Neural Information Processing Systems*, pages 2231–2239, 2012.

- [46] Y. Taigman, M. Yang, M. Ranzato, and L. Wolf. Deepface: Closing the gap to human-level performance in face verification. In *IEEE Conference on Computer Vision and Pattern Recognition*, pages 1701–1708, 2014.
- [47] P. Vincent, H. Larochelle, Y. Bengio, and P. Manzagol. Extracting and composing robust features with denoising autoencoders. In *ICML*, pages 1096–1103, 2008.
- [48] A. Wang, J. Cai, J. Lu, and T. Cham. MMSS: multi-modal sharable and specific feature learning for RGB-D object recognition. In *IEEE International Conference on Computer Vision*, pages 1125–1133, 2015.
- [49] X. Wang, D. F. Fouhey, and A. Gupta. Designing deep networks for surface normal estimation. In *IEEE Conference on Computer Vision and Pattern Recognition*, pages 539–547, 2015.
- [50] K. Xu, J. Ba, R. Kiros, K. Cho, A. C. Courville, R. Salakhutdinov, R. S. Zemel, and Y. Bengio. Show, attend and tell: Neural image caption generation with visual attention. In *International Conference on Machine Learning*, pages 2048–2057, 2015.